Editors' Suggestion | Featured in Physics

Long-Lived Coherence on a μHz Scale Optical Magnetic Quadrupole Transition

V. Klüsener,[1,2] S. Pucher,[1,2] D. Yankelev,[1,2,*] J. Trautmann,[1,2] F. Spriestersbach,[1,2] D. Filin,[3] S. G. Porsev,[3] M. S. Safronova,[3] I. Bloch,[1,4,2] and S. Blatt[1,4,2,†]

[1]*Max-Planck-Institut für Quantenoptik, 85748 Garching, Germany*
[2]*Munich Center for Quantum Science and Technology, 80799 München, Germany*
[3]*Department of Physics and Astronomy, University of Delaware, Newark, Delaware 19716, USA*
[4]*Fakultät für Physik, Ludwig-Maximilians-Universität München, 80799 München, Germany*

(Received 8 January 2024; accepted 29 April 2024; published 20 June 2024)

We report on the coherent excitation of the ultranarrow $^1S_0$–$^3P_2$ magnetic quadrupole transition in ^{88}Sr. By confining atoms in a state insensitive optical lattice, we achieve excitation fractions of 97(1)% and observe linewidths as narrow as 58(1) Hz. With Ramsey spectroscopy, we find coherence times of 14(1) ms, which can be extended to 266(36) ms using a spin-echo sequence. We determine the lifetime of the $^3P_2$ level for spontaneous emission of magnetic quadrupole radiation to be 110(31) min, confirming long-standing theoretical predictions. These results establish an additional clock transition in strontium and pave the way for applications of the metastable $^3P_2$ state in quantum computing and quantum simulations.

DOI: 10.1103/PhysRevLett.132.253201

The generation of long-lived coherences between atomic states on ultra-narrow optical transitions is fundamental for optical atomic clocks [1], quantum information processing [2–4], and quantum simulation [5,6].

The exceptional frequency resolution offered by such transitions provides the basis for the remarkable stability and precision of optical atomic clocks. Work on divalent systems has so far almost exclusively focused on the $^1S_0$–$^3P_0$ clock transition due to its insensitivity to environmental perturbations. As shown in Fig. 1(a), a complementary clock transition with μHz-scale natural linewidth is the $^1S_0$–$^3P_2$ magnetic quadrupole (M2) transition [7–10]. The interrogation of these two distinct clock transitions in the same atomic species can be advantageous for the evaluation of systematic shifts of the clock frequency [10–12], the search for physics beyond the standard model [13], and as a testbed for high precision atomic structure calculations [14].

Recently, clock transitions have found promising applications in quantum computing with atom arrays, where metastable clock states can serve as excellent qubits and present a gateway for high-fidelity two-qubit gates [2,3,15]. Single-qubit gates have been demonstrated on the $^1S_0$–$^3P_0$ transition in two-electron atoms and second-scale atomic coherence times have been observed [2,16]. Intriguingly, the combination of the metastable states $^3P_0$ and $^3P_2$ has been proposed for the implementation of a fast, high-fidelity qubit [17]. In combination with the ground state, the realization of an all-optical qutrit $^1S_0$–$^3P_0$–$^3P_2$ is conceivable [9].

Quantum simulation experiments with ultracold atoms also benefit from the exceptionally long coherence times and high frequency resolution provided by narrow optical transitions. Here, precision spectroscopy allows manipulating and probing quantum many-body systems at previously inaccessible energy scales [18,19]. Because the

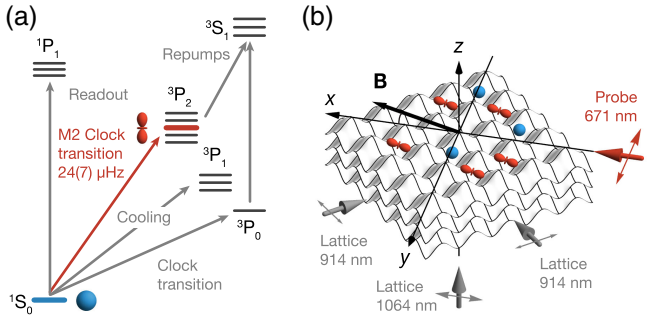

FIG. 1. Level scheme of ^{88}Sr and experimental setup. (a) Energy levels and transitions relevant for state preparation, spectroscopy, and detection. (b) Atoms are confined in a three-dimensional optical lattice at lattice wavelengths of 914 and 1064 nm for the horizontal and vertical axes, respectively. The polarizations of the lattice beams are adjusted to angles $\beta_{m,914}$ and $\beta_{m,1064}$ relative to the quantization axis defined by the magnetic field **B** in the xz plane. The probe laser propagates with wave vector **k** along the x axis and is linearly polarized along y perpendicular to the plane spanned by **k** and **B**.

nonspherical $^3P_2$ state possesses a nonzero *electric* quadrupole moment [20,21], it provides a new platform to study quantum gases with anisotropic, long-range quadrupole-quadrupole interactions [22,23].

For applications using ultracold atoms in metrology and quantum technology it is indispensable to preserve the inherently identical nature of the atoms by confining them in state insensitive optical potentials [24]. For the $^3P_2$ state, such "magic" trapping conditions can be achieved over an extensive range of trap wavelengths, spanning hundreds of nanometers by careful adjustment of the lattice polarization [9]. In particular, this tunability enables operating at trapping wavelengths where high power laser technology is available, thus significantly raising prospects for the scalability of neutral atom quantum technologies [25].

In this Letter, we generate long-lived atomic coherences by realizing the first coherent excitation of the ultranarrow $^1S_0$–$^3P_2$ M2 transition in ^{88}Sr. We demonstrate high-fidelity state preparation of the $^3P_2$ state, as well as high-resolution Rabi spectroscopy. The coherence properties of our system are systematically evaluated by performing Ramsey spectroscopy. Finally, we use the obtained spectroscopy results to determine the decay rate of the M2 transition. We compare our result to *ab initio* theoretical predictions, which have awaited experimental verification for more than two decades [20]. These results open up the metastable $^3P_2$ state for applications in metrology, quantum information processing, and quantum simulations.

Experimental sequence.—Our work starts by loading 2×10^5 ^{88}Sr atoms into a three-dimensional optical lattice. As shown in Fig. 1(b), the vertical lattice is formed by a retroreflected 1064-nm laser beam and the two horizontal lattice axes are generated by 914-nm laser beams inside an enhancement cavity [25]. The resulting three-dimensional optical lattice has a depth of $150E_{\mathrm{rec}}$ ($270E_{\mathrm{rec}}$) and trap frequency of 65 kHz (68 kHz) along the horizontal (vertical) axes, respectively, where $E_{\mathrm{rec}} = h^2/(2m\lambda_l^2)$ is the lattice photon recoil energy for an atom of mass m at the corresponding lattice wavelength λ_l and h denotes Planck's constant. The average occupation per lattice site is below unity and tunneling is negligible on experimental timescales such that strong inelastic collisions between atoms in the $^3P_2$ state can be avoided [26,27].

Despite the large disparity in wavelength of the different lattice axes, we achieve magic trapping conditions by matching the polarizability of the excited state $|e\rangle = |^3P_2, m_J = 0\rangle$ to the ground state $|g\rangle = |^1S_0\rangle$. While the polarizability of $|g\rangle$ is solely determined by λ_l, the polarizability of the nonspherical state $|e\rangle$ can be tuned via the angle β between linear lattice polarisation and quantization axis according to [28,29]

$$\alpha(\lambda_l, \beta) = \alpha_s(\lambda_l) - \alpha_t(\lambda_l)\frac{3\cos^2\beta - 1}{2}, \tag{1}$$

where α_s and α_t denote scalar and tensor polarizabilites, respectively. In our experiment, the quantization axis is defined by a 28 G bias magnetic field $\mathbf{B}$ angled at the measured "magic angle" $\beta_{m,1064} = 16(2)°$ with respect to the polarization of the 1064-nm vertical lattice [9]. For the 914-nm lattices we find magic trapping conditions close to the theoretically predicted angle $\beta_{m,914} = 52°$ (see Supplemental Material [30]).

After transferring the atoms to the lattice, we apply resolved sideband cooling on the $^1S_0$–$^3P_1$ transition. The resulting temperature of 2.3 μK (2.1 μK) corresponds to an average phonon occupation of $\bar{n} = 0.35$ (0.27) and a ground state fraction of 74% (79%) along the probe (vertical) axis.

To interrogate the $^1S_0$–$^3P_2$ M2 transition, we apply a 671 nm probe beam propagating with wave-vector $\mathbf{k}$ along the horizontal x axis. We use probe powers of up to 50 mW and a $1/e^2$ beam waist radius of 500 μm, much larger than the sample size of about 50 μm. The linewidth of the frequency-stabilized probe laser is on the Hertz level [30]. Its polarization $\boldsymbol{\epsilon}$ is chosen to be linear and is oriented orthogonal to the plane spanned by $\mathbf{k}$ and $\mathbf{B}$. We note that this choice of polarization excludes excitation of the $^1S_0$–$^3P_2$ transition as an electric-dipole (E1) transition induced via magnetic field admixing [36].

Following the spectroscopy sequence, we read out the number of $|g\rangle$ atoms through absorption imaging on the $^1S_0$–$^1P_1$ transition. Alternatively, after removal of $|g\rangle$ atoms, the number of $|e\rangle$ atoms is measured by repumping atoms to $|g\rangle$ via the $^3S_1$ state and taking an absorption image [see Fig. 1(a)]. Populations are obtained via normalization to interleaved reference measurements of the total atom number [30].

Rabi spectroscopy.—The realization of a state-insensitive trap allows us to perform precision spectroscopy on the ultranarrow M2 transition. We coherently excite atoms to $|e\rangle$ by performing Rabi spectroscopy. Upon applying square probe pulses of varying pulse duration, we observe coherent oscillations of the atomic state populations, as shown in Fig. 2(a) for a Rabi frequency of $\Omega = 2\pi \times 189(1)$ Hz. For a 2.6 ms-long resonant π pulse we observe an excitation fraction of 97(1)%.

In Fig. 2(b), we show Rabi spectra obtained for two different probe beam intensities. We adjust the probe pulse duration to perform excitation with a π pulse when on resonance. For pulse durations of 2.6 and 15 ms, we observe spectra with 370(2) and 58(1) Hz full width at half maximum (FWHM), respectively. The minimum achievable linewidth is limited by residual lattice light shifts and eventually by the finite linewidth of the probe laser. In addition to the difference in linewidths, we also observe a shift in the resonance frequency for different probe beam intensities. This probe-light-induced differential ac Stark shift Δ_{ac} arises due to off-resonant coupling of the probe light to additional states [36].

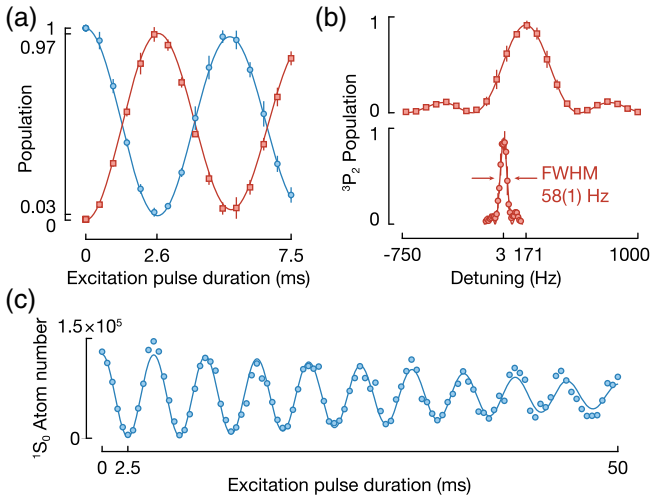

FIG. 2. Rabi spectroscopy. (a) Rabi oscillations of the $|g\rangle$ (blue circles) and $|e\rangle$ (red squares) populations for varying excitation times. Solid lines are fits to a sinusoidal oscillation with Gaussian damping. From the amplitudes of the fits we extract a maximum excitation fraction of 97(1)%. (b) Spectra obtained for π pulse durations of 2.6 (top) and 15 ms (bottom). Solid lines show fits to a Rabi line shape with FWHM of 370(2) and 58(1) Hz, respectively. We observe a probe-light-induced Stark shift of the line center and set the zero of the frequency axis to the unshifted transition frequency. (c) Long-term evolution of Rabi oscillations displaying motional dephasing due to the finite temperature of the atomic sample. The solid line shows a fit to a sinusoidal oscillation with Gaussian damping, yielding a $1/e$ decay time of 57(5) ms.

The long-term evolution of Rabi oscillations at a fitted Rabi frequency of $\Omega = 2\pi \times 200(1)$ Hz is shown in Fig. 2(c). We observe damping with a $1/e$ timescale of 57(5) ms, limited predominantly by motional dephasing due to the finite temperature and confinement of the atomic sample along the interrogation axis. This dephasing arises because after sideband cooling several vibrational states remain populated and the carrier Rabi frequency depends on the vibrational state [37,38]. Other effects that contribute to the dephasing are residual lattice light shifts, intensity fluctuations of the probe beam, and spatial inhomogeneities (see Supplemental Material [30]).

Ramsey spectroscopy.—To characterize the atom-atom coherence of the prepared states we perform Ramsey spectroscopy and optionally add a spin-echo pulse, as sketched in Fig. 3(a). For Ramsey spectroscopy, we apply a $\pi/2$ pulse of duration $T_\pi/2 = 1.3$ ms to prepare a coherent superposition state $(|g\rangle + |e\rangle)/\sqrt{2}$, which evolves to $(|g\rangle + e^{-i\phi}|e\rangle)/\sqrt{2}$ by acquiring a relative phase shift ϕ during the free evolution time T. Finally, we map this phase difference into a population difference by applying another $\pi/2$ pulse to obtain the state $(i\sin\phi|g\rangle + \cos\phi|e\rangle)/\sqrt{2}$ [39]. In our experiment, the acquired phase is proportional to the probe-light-induced Stark shift Δ_{ac}. For the probe intensity used in Fig. 3, the resulting Ramsey signal oscillates at about 140 Hz. The oscillations exhibit a Gaussian decay indicating an inhomogeneous distribution of detunings, leading to the loss of atom-atom coherence. We also observe this contrast decay for Ramsey fringes as a function of detuning for increasing T, as shown in Fig. 3(d).

To quantify these results, we measure the decay of the Ramsey contrast when scanning the phase of the final $\pi/2$ pulse for varying T in Fig. 3(e). We extract an inhomogeneous dephasing time $T_2^* = 14(1)$ ms, indicating a Gaussian distribution of detunings with a standard deviation of $\sqrt{2}/T_2^* = 2\pi \times 16(1)$ Hz [2]. This inhomogenous distribution can be mainly attributed to residual light shifts of the optical lattice and sets a limit for the most narrow observable spectra [30].

Next, we demonstrate that dephasing of the atom-atom coherence due to lattice light shifts can be reversed to a large extent through the application of a spin-echo sequence [40]. To this end, we extend the spectroscopy sequence by an additional π pulse of duration T_π after a free evolution time $T/2$ [see Fig. 3(a)]. In Figs. 3(b) and 3(c) we observe rephasing of the atomic spins in the form of a spin echo at time T by scanning the timing of the final $\pi/2$ pulse. For evolution times within the coherence time of our clock laser, we observe spin-echo signals that feature coherent oscillations. Even after atom-laser coherence is lost, we still observe variance in the spin-echo signal for longer evolution times. This confirms the presence of atom-atom coherence, which is now probed with a random phase of the clock laser [16]. From the Gaussian decay of phase contrast measurements shown in Fig. 3(e) we infer a homogeneous dephasing time $T_2' = 266(36)$ ms [40], presumably limited by fluctuations of the quantization axis angle and of the lattice polarizations [30]. For even longer evolution times, we start to observe the finite excited-state trap lifetime with a $1/e$ timescale of 5 s due to trap-induced Raman scattering [41] and the onset of tunneling leading to collisional loss of atoms in $|e\rangle$ [26,27].

Transition strength.—Finally, we use the obtained spectroscopic results to determine the decay rate A_{M2} for spontaneous emission of a magnetic quadrupole photon. Simultaneous measurement of the Rabi frequency Ω along with the probe light shift Δ_{ac} allows for an accurate determination of the transition strength insensitive to the probe beam intensity. Following Lange *et al.* [44], we define the probe-intensity-independent quantity $\xi = \Omega^2/\Delta_{\mathrm{ac}}$, called the relative excitation strength. In Fig. 4, we plot Ω and Δ_{ac} for different intensity settings of the probe beam. From a nonlinear fit to this data we extract a relative excitation strength $\xi = 2\pi \times 283(12)$ Hz [30].

We combine ξ with the differential polarizability $\Delta\alpha_{\mathrm{eg}}(\nu_0)$ at the transition frequency ν_0 and determine the transition rate [30,44] as

$$A_{\mathrm{M2}} = \frac{8\pi\nu_0^3}{5\epsilon_0 c^3}\Delta\alpha_{\mathrm{eg}}(\nu_0)\xi\frac{1}{6\cos^2\theta\sin^2\theta}, \tag{2}$$

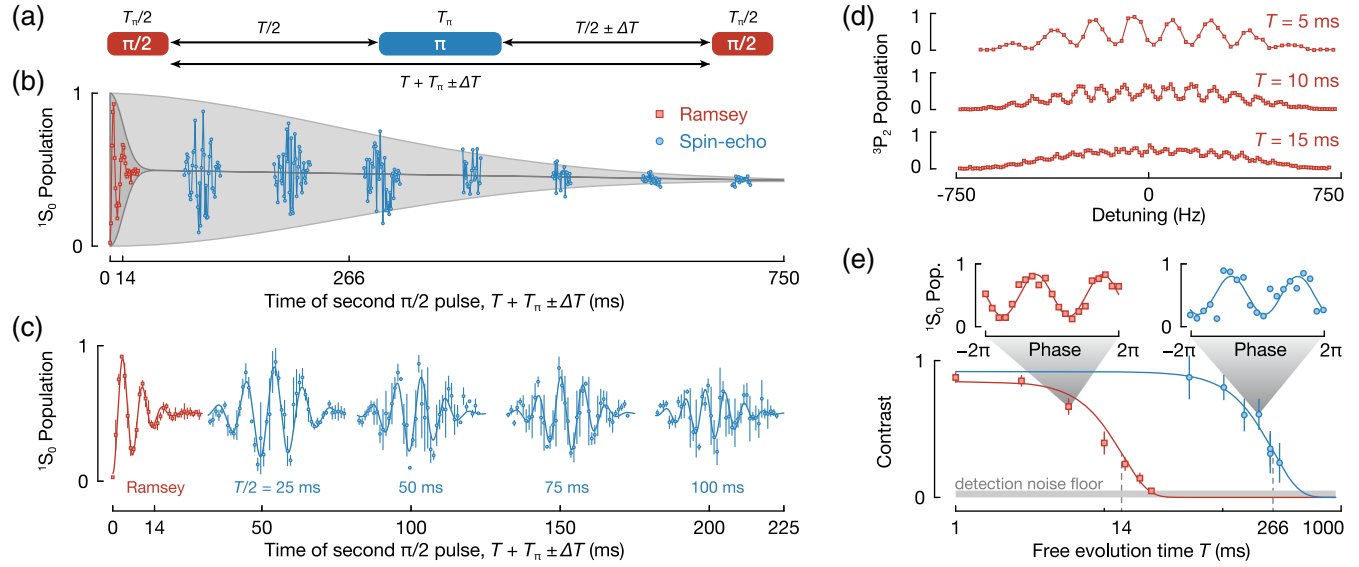

FIG. 3. Ramsey spectroscopy. (a) Illustration of pulse sequences employed for Ramsey and spin-echo experiments. (b) Ramsey (red squares) and spin-echo (blue circles) signals from single experimental runs. The dark (light) gray shaded regions represent a Gaussian decay of the Ramsey (spin-echo) contrast combined with an exponential decay to account for finite atom lifetime in the lattice. (c) Ramsey and spin-echo signals averaged over three experimental runs. The solid lines represent fits to a sinusoidal oscillation with Gaussian envelope to guide the eye. (d) Ramsey fringes for free evolution times T of 5, 10, and 15 ms (from top to bottom). (e) Contrast decay of the Ramsey (red squares) and spin-echo (blue circles) signals for different free evolution times T. The gray-shaded area denotes the detection noise floor of our system set by atom number fluctuations and the insets show Ramsey and spin-echo phase scans. The solid lines represent Gaussian fits to the contrast decay, with $1/e$ decay times of 14(1) and 266(36) ms for Ramsey and spin-echo sequences, respectively, leading to the gray-shaded areas in panel (b).

where ϵ_0 is the vacuum permittivity and c is the speed of light. The last term models the geometry of the probe beam propagating at an angle θ relative to the quantization axis with linear polarization perpendicular to the plane spanned by $\mathbf{k}$ and $\mathbf{B}$ [45]. For the differential polarizability at the transition frequency, we use the theory value $\Delta\alpha_{\mathrm{eg}}(\nu_0) = 290(7)$ a.u. [30]. Using these results with our experimental angle $\theta = 14(2)°$ [30] and the absolute transition frequency ν_0 [9], the decay rate of the M2 transition in ^{88}Sr is

$$A_{\mathrm{M2}} = 152(43) \times 10^{-6}\ \mathrm{s}^{-1}, \tag{3}$$

corresponding to a transition linewidth $A_{\mathrm{M2}}/(2\pi) = 24(7)$ μHz and a lifetime for emission of magnetic quadrupole radiation of $A_{\mathrm{M2}}^{-1} = 110(31)$ min. The uncertainty is dominated by uncertainties in the angle θ [30].

We stress that to obtain the total lifetime of the $^3P_2$ state, other relevant decay channels have to be considered. In particular, magnetic dipole (M1) decay to $^3P_1$ and blackbody-radiation-induced quenching to $4d\,^3\mathrm{D}_J$ states are expected to contribute significantly at room temperature [20,46].

In Fig. 4(c), we compare our experimentally measured transition rate to a new *ab initio* calculation and to theory predictions from the literature [20,21,42,43]. To calculate A_{M2} we use a hybrid approach combining configuration interaction (CI) and coupled cluster (CC) methods [14]. The CI computation includes an interaction between the two valence electrons of strontium while the coupled cluster method accounts for core-core and core-valence correlations. The wave functions Φ_n and energy levels E_n of the valence electrons are found by solving the

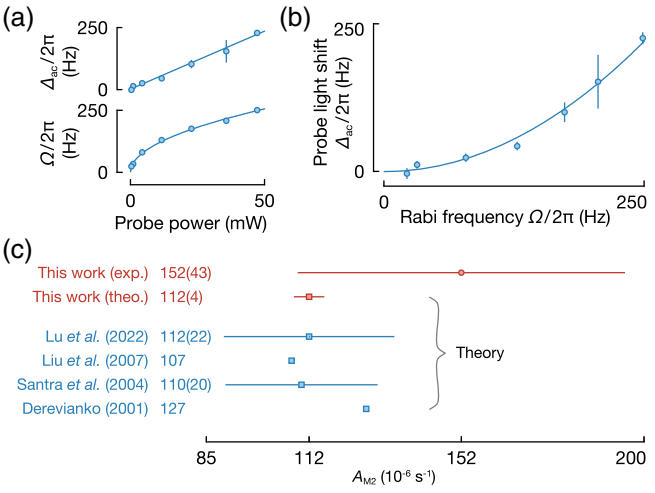

FIG. 4. Evaluation of M2 transition rate. (a) Measured probe light shifts Δ_{ac} (top) and Rabi frequencies Ω (bottom) for different probe beam powers. Solid lines are fits denoting a linear and square root scaling, respectively. (b) From a nonlinear fit of the form $\Delta_{\mathrm{ac}} = \xi^{-1}\Omega^2$ with reduced χ^2 of 1.1 we extract the relative excitation strength $\xi = 2\pi \times 283(12)$ Hz. (c) Comparison of experimental (circle) and theoretical (squares) values of the decay rate AM_2 [20,21,42,43].

multiparticle relativistic equation $H_{\mathrm{eff}}(E_n)\Phi_n = E_n\Phi_n$ [47], where the effective Hamiltonian is defined as $H_{\mathrm{eff}}(E) = H_{\mathrm{FC}} + \Sigma(E)$ with the Hamiltonian H_{FC} in the frozen-core approximation. The energy-dependent operator $\Sigma(E)$ accounts for virtual excitations of the core electrons. To quantify uncertainties, which arise from incomplete inclusion of the core, we carry out several computations, which include the core, i.e., build the $\Sigma(E)$ operator, in different approximations (see Supplemental Material [30]). As a result, we estimate the absolute value of the M2 $\langle {}^1S_0 \| \mathrm{M2} \| {}^3P_2 \rangle$ matrix element to $22.6(4)\mu_B$ with 2% total uncertainty and the M2 transition rate to $112(4) \times 10^{-6}$ s^{-1} with 4% uncertainty. Here, μ_B denotes the Bohr magneton.

Summary and outlook.—We have demonstrated that the ${}^1S_0$–${}^3P_2$ M2 transition can be coherently controlled with high frequency resolution. Excitation to the ${}^3P_2$ state is possible with high fidelity and we have observed hundreds of milliseconds long coherence times, despite the higher sensitivity to environmental perturbations of the ${}^3P_2$ state compared to the well-established ${}^3P_0$ state. These results enable applications of the ${}^3P_2$ state in quantum information processing [17]. Further improvements in pulse fidelities and coherence times are expected by improved cooling or by employing robust qubit rotation and dynamical decoupling schemes [48]. Reaching lower temperatures will also enable operation at lower trap depths where lattice light shifts are even further reduced. With the obtained advances in spectral resolution, many energy scales of quantum many-body systems, such as tunneling dynamics or contact interactions, can now be probed on the M2 transition. The study of long-range quadrupolar interactions between ultracold atoms in the ${}^3P_2$ state, which give rise to frequency shifts on the Hertz level, is now within reach [22,23]. Our results establish an additional clock transition in strontium, demonstrate the suitability of the ${}^3P_2$ state for a qubit, and pave the way for a unique new quantum simulation platform based on nonspherical atoms.

Note added.—In recent work, the ${}^3P_2$ state has been used to encode a fine-structure qubit in ^{88}Sr and magic-angle traps have been used to achieve extended qubit coherence times [49,50].

We thank A. Derevianko for stimulating discussions, S. Snigirev and Y. Yang for support with experimental software and hardware, and A. Schindewolf and J. Geiger for careful reading of the manuscript. The Munich team acknowledges funding by the Munich Quantum Valley initiative as part of the High-Tech Agenda Plus of the Bavarian State Government, by the BMBF through the program "Quantum technologies—from basic research to market" (Grant No. 13N16357), and funding under the Horizon Europe program HORIZON-CL4-2022-QUANTUM-02-SGA via the project 101113690 (PASQuanS2.1). The Delaware team's research was supported in part by the U.S. Office of Naval Research (Grant No. N00014-20-1-2513), the European Research Council (ERC) under the European Union's Horizon 2020 research and innovation program (Grant No. 856415), and the U.S. NSF QLCI Grant No. OMA–2016244 and through the use of University of Delaware HPC Caviness and DARWIN computing systems. V. K. thanks the Hector Fellow Academy for support.

*Present address: Rafael Ltd., Haifa 3102102, Israel.
†sebastian.blatt@mpq.mpg.de

[1] A. D. Ludlow, M. M. Boyd, J. Ye, E. Peik, and P. O. Schmidt, Optical atomic clocks, Rev. Mod. Phys. **87**, 637 (2015).
[2] I. S. Madjarov, J. P. Covey, A. L. Shaw, J. Choi, A. Kale, A. Cooper, H. Pichler, V. Schkolnik, J. R. Williams, and M. Endres, High-fidelity entanglement and detection of alkaline-earth Rydberg atoms, Nat. Phys. **16**, 857 (2020).
[3] J. W. Lis, A. Senoo, W. F. McGrew, F. Rönchen, A. Jenkins, and A. M. Kaufman, Mid-circuit operations using the *omg* architecture in neutral atom arrays, Phys. Rev. X **13**, 041035 (2023).
[4] H. Häffner, C. F. Roos, and R. Blatt, Quantum computing with trapped ions, Phys. Rep. **469**, 155 (2008).
[5] C. Gross and I. Bloch, Quantum simulations with ultracold atoms in optical lattices, Science **357**, 995 (2017).
[6] C. Roos and R. Blatt, Quantum simulations with trapped ions, Nat. Phys. **8**, 277 (2012).
[7] A. Yamaguchi, S. Uetake, S. Kato, H. Ito, and Y. Takahashi, High-resolution laser spectroscopy of a Bose-Einstein condensate using the ultranarrow magnetic quadrupole transition, New J. Phys. **12**, 103001 (2010).
[8] O. Onishchenko, S. Pyatchenkov, A. Urech, C.-C. Chen, S. Bennetts, G. A. Siviloglou, and F. Schreck, Frequency of the ultranarrow ${}^1S_0$–${}^3P_2$ transition in ^{87}Sr, Phys. Rev. A **99**, 052503 (2019).
[9] J. Trautmann, D. Yankelev, V. Klüsener, A. J. Park, I. Bloch, and S. Blatt, ${}^1S_0 - {}^3P_2$ magnetic quadrupole transition in neutral strontium, Phys. Rev. Res. **5**, 013219 (2023).
[10] M. A. Bohman, S. G. Porsev, D. B. Hume, D. R. Leibrandt, and M. S. Safronova, Enhancing divalent optical atomic clocks with the ${}^1S_0 \leftrightarrow {}^3P_2$ transition, Phys. Rev. A **108**, 053120 (2023).
[11] H. A. Fürst, C.-H. Yeh, D. Kalincev, A. P. Kulosa, L. S. Dreissen, R. Lange, E. Benkler, N. Huntemann, E. Peik, and T. E. Mehlstäubler, Coherent excitation of the highly forbidden electric octupole transition in ^{172}Yb$^+$, Phys. Rev. Lett. **125**, 163001 (2020).
[12] T. Zanon-Willette, F. Impens, E. Arimondo, D. Wilkowski, A. V. Taichenachev, and V. I. Yudin, Engineering quantum control with optical transitions induced by twisted light fields, Phys. Rev. A **108**, 043513 (2023).
[13] V. A. Dzuba, V. V. Flambaum, and S. Schiller, Testing physics beyond the standard model through additional clock transitions in neutral ytterbium, Phys. Rev. A **98**, 022501 (2018).
[14] M. S. Safronova, M. G. Kozlov, W. R. Johnson, and D. Jiang, Development of a configuration-interaction plus

all-order method for atomic calculations, Phys. Rev. A **80**, 012516 (2009).
[15] D. Okuno, Y. Nakamura, T. Kusano, Y. Takasu, N. Takei, H. Konishi, and Y. Takahashi, High-resolution spectroscopy and single-photon Rydberg excitation of reconfigurable ytterbium atom tweezer arrays utilizing a metastable state, J. Phys. Soc. Jpn. **91**, 084301 (2022).
[16] A. W. Young, W. J. Eckner, W. R. Milner, D. Kedar, M. A. Norcia, E. Oelker, N. Schine, J. Ye, and A. M. Kaufman, Half-minute-scale atomic coherence and high relative stability in a tweezer clock, Nature (London) **588**, 408 (2020).
[17] A. Pagano, S. Weber, D. Jaschke, T. Pfau, F. Meinert, S. Montangero, and H. P. Büchler, Error budgeting for a controlled-phase gate with strontium-88 Rydberg atoms, Phys. Rev. Res. **4**, 033019 (2022).
[18] X. Zhang, M. Bishof, S. L. Bromley, C. V. Kraus, M. S. Safronova, P. Zoller, A. M. Rey, and J. Ye, Spectroscopic observation of SU(N)-symmetric interactions in Sr orbital magnetism, Science **345**, 1467 (2014).
[19] S. Kato, K. Inaba, S. Sugawa, K. Shibata, R. Yamamoto, M. Yamashita, and Y. Takahashi, Laser spectroscopic probing of coexisting superfluid and insulating states of an atomic Bose-Hubbard system, Nat. Commun. **7**, 11341 (2016).
[20] A. Derevianko, Feasibility of cooling and trapping metastable alkaline-earth atoms, Phys. Rev. Lett. **87**, 023002 (2001).
[21] R. Santra, K. V. Christ, and C. H. Greene, Properties of metastable alkaline-earth-metal atoms calculated using an accurate effective core potential, Phys. Rev. A **69**, 042510 (2004).
[22] S. G. Bhongale, L. Mathey, E. Zhao, S. F. Yelin, and M. Lemeshko, Quantum phases of quadrupolar Fermi gases in optical lattices, Phys. Rev. Lett. **110**, 155301 (2013).
[23] M. Lahrz, M. Lemeshko, K. Sengstock, C. Becker, and L. Mathey, Detecting quadrupole interactions in ultracold Fermi gases, Phys. Rev. A **89**, 043616 (2014).
[24] H. Katori, M. Takamoto, V. G. Pal'chikov, and V. D. Ovsiannikov, Ultrastable optical clock with neutral atoms in an engineered light shift trap, Phys. Rev. Lett. **91**, 173005 (2003).
[25] A. J. Park, J. Trautmann, N. Šantić, V. Klüsener, A. Heinz, I. Bloch, and S. Blatt, Cavity-enhanced optical lattices for scaling neutral atom quantum technologies to higher qubit numbers, PRX Quantum **3**, 030314 (2022).
[26] A. Traverso, R. Chakraborty, Y. N. Martinez de Escobar, P. G. Mickelson, S. B. Nagel, M. Yan, and T. C. Killian, Inelastic and elastic collision rates for triplet states of ultracold strontium, Phys. Rev. A **79**, 060702(R) (2009).
[27] Ch. Lisdat, J. S. R. V. Winfred, T. Middelmann, F. Riehle, and U. Sterr, Collisional losses, decoherence, and frequency shifts in optical lattice clocks with bosons, Phys. Rev. Lett. **103**, 090801 (2009).
[28] F. Le Kien, P. Schneeweiss, and A. Rauschenbeutel, Dynamical polarizability of atoms in arbitrary light fields: General theory and application to cesium, Eur. Phys. J. D **67**, 92 (2013).
[29] A. Heinz, A. J. Park, N. Šantić, J. Trautmann, S. G. Porsev, M. S. Safronova, I. Bloch, and S. Blatt, State-dependent optical lattices for the strontium optical qubit, Phys. Rev. Lett. **124**, 203201 (2020).
[30] See Supplemental Material at http://link.aps.org/supplemental/10.1103/PhysRevLett.132.253201 for detailed methods and additional information, which includes Refs. [31–35].
[31] S. G. Porsev, M. S. Safronova, and M. G. Kozlov, Precision calculation of hyperfine constants for extracting nuclear moments of ^{229}Th, Phys. Rev. Lett. **127**, 253001 (2021).
[32] V. A. Dzuba, V. V. Flambaum, M. G. Kozlov, and S. G. Porsev, Using effective operators in calculating the hyperfine structure of atoms, Sov. J. Exp. Theor. Phys. **87**, 885 (1998).
[33] S. G. Porsev, Y. G. Rakhlina, and M. G. Kozlov, Electric-dipole amplitudes, lifetimes, and polarizabilities of the low-lying levels of atomic ytterbium, Phys. Rev. A **60**, 2781 (1999).
[34] S. G. Porsev, Y. G. Rakhlina, and M. G. Kozlov, Calculation of hyperfine structure constants for ytterbium, J. Phys. B **32**, 1113 (1999).
[35] A. Kramida, Yu. Ralchenko, J. Reader, and NIST ASD Team, NIST Atomic Spectra Database (version 5.11), [Online]. Available: https://physics.nist.gov/asd National Institute of Standards and Technology, Gaithersburg, MD (2023).
[36] A. V. Taichenachev, V. I. Yudin, C. W. Oates, C. W. Hoyt, Z. W. Barber, and L. Hollberg, Magnetic field-induced spectroscopy of forbidden optical transitions with application to lattice-based optical atomic clocks, Phys. Rev. Lett. **96**, 083001 (2006).
[37] S. Blatt, J. W. Thomsen, G. K. Campbell, A. D. Ludlow, M. D. Swallows, M. J. Martin, M. M. Boyd, and J. Ye, Rabi spectroscopy and excitation inhomogeneity in a one-dimensional optical lattice clock, Phys. Rev. A **80**, 052703 (2009).
[38] A. M. Kaufman, B. J. Lester, and C. A. Regal, Cooling a single atom in an optical tweezer to its quantum ground state, Phys. Rev. X **2**, 041014 (2012).
[39] G. E. Marti, R. B. Hutson, A. Goban, S. L. Campbell, N. Poli, and J. Ye, Imaging optical frequencies with 100 μHz precision and 1.1 μm resolution, Phys. Rev. Lett. **120**, 103201 (2018).
[40] S. Kuhr, W. Alt, D. Schrader, I. Dotsenko, Y. Miroshnychenko, A. Rauschenbeutel, and D. Meschede, Analysis of dephasing mechanisms in a standing-wave dipole trap, Phys. Rev. A **72**, 023406 (2005).
[41] S. Dörscher, R. Schwarz, A. Al-Masoudi, S. Falke, U. Sterr, and C. Lisdat, Lattice-induced photon scattering in an optical lattice clock, Phys. Rev. A **97**, 063419 (2018).
[42] Y. Liu, M. Andersson, T. Brage, Y. Zou, and R. Hutton, Lifetime calculations for the $5s5p\,^3P_2$ metastable level of ^{88}Sr I, Phys. Rev. A **75**, 014502 (2007).
[43] B. Lu, X. Lu, J. Li, and H. Chang, Reconciliation of theoretical lifetimes of the 5s5p metastable state for ^{88}Sr with measurement: The role of the blackbody-radiation-induced decay, Chin. Phys. Lett. **39**, 073201 (2022).
[44] R. Lange, A. A. Peshkov, N. Huntemann, C. Tamm, A. Surzhykov, and E. Peik, Lifetime of the $^2F_{7/2}$ level in Yb$^+$ for spontaneous emission of electric octupole radiation, Phys. Rev. Lett. **127**, 213001 (2021).
[45] S. A.-L. Schulz, A. A. Peshkov, R. A. Müller, R. Lange, N. Huntemann, Chr. Tamm, E. Peik, and A. Surzhykov,

Generalized excitation of atomic multipole transitions by twisted light modes, Phys. Rev. A **102**, 012812 (2020).

[46] M. Yasuda and H. Katori, Lifetime measurement of the $^3P_2$ metastable state of strontium atoms, Phys. Rev. Lett. **92**, 153004 (2004).

[47] V. A. Dzuba, V. V. Flambaum, and M. G. Kozlov, Combination of the many-body perturbation theory with the configuration-interaction method, Phys. Rev. A **54**, 3948 (1996).

[48] D. Bluvstein, H. Levine, G. Semeghini, T. T. Wang, S. Ebadi, M. Kalinowski, A. Keesling, N. Maskara, H. Pichler, M. Greiner, V. Vuletić, and M. D. Lukin, A quantum processor based on coherent transport of entangled atom arrays, Nature (London) **604**, 451 (2022).

[49] G. Unnikrishnan, P. Ilzhöfer, A. Scholz, C. Hölzl, A. Götzelmann, R. K. Gupta, J. Zhao, J. Krauter, S. Weber, N. Makki, H. P. Büchler, T. Pfau, and F. Meinert, Coherent control of the fine-structure qubit in a single alkaline-earth atom, Phys. Rev. Lett. **132**, 150606 (2024).

[50] S. Pucher, V. Klüsener, F. Spriestersbach, J. Geiger, A. Schindewolf, I. Bloch, and S. Blatt, Fine-structure qubit encoded in metastable strontium trapped in an optical lattice, Phys. Rev. Lett. **132**, 150605 (2024).